Localization and cross section reconstruction of fluorescent targets in *ex vivo* breast tissue using independent component analysis

M. Alrubaiee,[a] M. Xu, S. K. Gayen, and R. R. Alfano
Institute for Ultrafast Spectroscopy and Lasers, Physics Department, The City College of New York of the City University of New York, 138th Street, Convent Avenue, New York, New York 10031

(Received 21 February 2006; accepted 24 July 2006; published online 27 September 2006)

An information theory based approach is introduced for the detection and three-dimensional localization of fluorescent targets embedded in a turbid medium. The approach uses multisource illumination of the medium, multidetector transillumination acquisition of fluorescence signal, independent component analysis for target detection and localization, and a back-projection algorithm for reconstruction of target cross section. The efficacy of the approach is demonstrated by locating and estimating the cross section of a fluorescent target embedded in a $100\times100\times26\ \mathrm{mm}^3$ *ex vivo* human breast tissue specimen and in a tissue-simulating turbid medium of thickness 50 times the transport mean free path. © *2006 American Institute of Physics*. [DOI: 10.1063/1.2356024]

Development of optical fluorescence tomography is of interest for cancer detection and diagnosis.[1–4] The recent advent of fluorescence beacons and contrast agents with the ability to attach themselves to desired abnormal cells or organelles[5] enhances the target specificity and diagnostic potential of fluorescence based optical imaging approaches. Determination of accurate location of targets embedded in a turbid medium remains a formidable task for both direct imaging and inverse image reconstruction approaches and for all types of targets—fluorescent, absorptive, and scattering.[6–11] We have introduced an approach, known as optical tomography using independent component analysis (OPTICA), that enables more accurate determination of target location in turbid media than existing optical methods.[12,13] It uses multisource optical probing of the sample, multidetector acquisition of transmitted signal, and independent component analysis[14] of information theory to analyze the signal for three-dimensional (3D) localization and characterization of the target. The efficacy of OPTICA for locating small absorptive and scattering targets embedded in turbid media has been demonstrated.[11,15] In this letter, OPTICA formalism is extended for fluorescent targets, and its efficacy is tested by obtaining 3D location and cross sectional image of a fluorescent target in an *ex vivo* human breast tissue sample and in a tissue-simulating turbid medium from experimental data.

The theoretical formalism for fluorescence OPTICA is based on the premise that the spatial distribution of the light intensity at the exit boundary of the medium is a weighted mixture of signals arriving from the fluorescent targets ("sources") embedded in the medium:

$$x(\mathbf{r}_d,\mathbf{r}_s)=\sum_j a_j(\mathbf{r}_d)s_j(\mathbf{r}_s), \tag{1}$$

where $a_j(\mathbf{r}_d)$ is the mixing vector and $a_j(\mathbf{r}_d)s_j(\mathbf{r}_s)$ represents the contribution of the jth target to the fluorescent signal at the detector plane for illumination of the source plane at $\mathbf{r}_s$. Independent component analysis assumes that these fluorescent sources are independent, treats the problem of detecting those as a source separation problem, and obtains a_j and s_j by seeking maximal mutual independence between s_j's.[12,14]

Light propagation in a highly scattering medium with an embedded fluorescent target excited by an external light source is approximately described by coupled diffusion equations at the excitation and emission wavelengths.[16,17] The fluorescence signal $U_m(\mathbf{r}_d,\mathbf{r}_s,\omega)$ can be expressed in terms of the two Green's functions $G_x(\mathbf{r},\mathbf{r}_s,\omega)$ and $G_m(\mathbf{r}_d,\mathbf{r},\omega)$ describing light propagation from the excitation source at $\mathbf{r}_s$ to the fluorescent target at $\mathbf{r}$ at the excitation wavelength λ_x and the light propagation from the target to the detector at $\mathbf{r}_d$ at the emission wavelength λ_m. In this letter we report on slab samples. Consequently, Green's functions for a slab geometry[18] under the diffusion approximation of the equation of radiative transfer are used.

Assuming that the jth fluorescent target is contained in volume V_j centered at $\mathbf{r}_j$, the fluorescence signal under excitation by a unit point source at $\mathbf{r}_s$ is given by

$$U_m(\mathbf{r}_d,\mathbf{r}_s,\omega)=\sum_{j=1}^{j} G_m(\mathbf{r}_d,\mathbf{r}_j,\omega)f_j(\omega)G_x(\mathbf{r}_j,\mathbf{r}_s,\omega), \tag{2}$$

where $f_j(\omega)=\gamma(\mathbf{r}_j)cV_j/[1-i\omega\tau(\mathbf{r}_j)]$ represents the fluorescence signal strength of the jth target, γ is the fluorescent yield, c is the speed of light in medium, τ is the fluorescence lifetime, and ω is the angular modulation frequency of the excitation light intensity.

Both the location and the strength of the jth target can be computed by using a least square fitting procedure:

$$\min_{\mathbf{r}_j,\alpha_j,\beta_j}\left\{\sum_{r_s}[\alpha_j^{-1}s_j(\mathbf{r}_s)-G_x(\mathbf{r}_j,\mathbf{r}_s)]^2+\sum_{r_d}[\beta_j^{-1}a_j(\mathbf{r}_d)-G_m(\mathbf{r}_d,\mathbf{r}_j)]^2\right\}, \tag{3}$$

where $s_j(\mathbf{r}_s)\propto G_x(\mathbf{r}_j,\mathbf{r}_s,\omega)$ and $a_j(\mathbf{r}_d)\propto G_m(\mathbf{r}_d,\mathbf{r}_j,\omega)$. The fitting yields the location $\mathbf{r}_j$ of and the two scaling constants α_j and β_j for the jth target. The fluorescence strength then is $f_j=\alpha_j\beta_j$.

The size and shape of the jth target can be estimated from a back projection of $U_{m_j}(\mathbf{r}_d,\mathbf{r}_s,\omega)$ from the detection plane onto the "target plane," i.e., $z=z_j$ plane. The fluorescence signal from the jth target is approximated by

[a]Electronic mail: malrub@sci.ccny.cuny.edu

$$U_{m_j}(\mathbf{r}_d, \mathbf{r}_s, \omega) = \int G_m(\boldsymbol{\rho}_d - \boldsymbol{\rho}, \omega) X_j(\boldsymbol{\rho}) G_x(\boldsymbol{\rho} - \boldsymbol{\rho}_s, \omega) d\boldsymbol{\rho}, \tag{4}$$

where the integration is over the $z=z_j$ plane and $\boldsymbol{\rho}_d$ and $\boldsymbol{\rho}_s$ are the lateral coordinates of the detector and the source, respectively. In the Fourier space, $X_j(\mathbf{q})$ can be obtained from Eq. (4) as

$$X_j(\mathbf{q}) = \frac{U_{m_j}(\mathbf{q} - \mathbf{q}_s, \mathbf{q}_s, \omega)}{G_m(\mathbf{q} - \mathbf{q}_s, \omega) G_x^*(\mathbf{q}_s, \omega)}, \tag{5}$$

where $\mathbf{q}$ and $\mathbf{q}_s$ are the spatial frequencies on the x-y plane and * denotes complex conjugate. The inverse Fourier transforms of $X_j(\mathbf{q})$ yield the cross sectional image of the fluorescent target in the $z=z_j$ plane. The full width at half maximum (FWHM) of the cross sectional image provides an estimate of the real target size. The cross sectional image is a two-dimensional (2D) distribution of the fluorescent object at the target plane.

The experimental arrangement to test the fluorescence OPTICA approach is shown schematically in Fig. 1(a). The fluorescent target was a glass sphere (outer diameter of ~4 mm and inner diameter of 3.2 mm) filled with a solution of indocyanine green (ICG) in water. The water solution of ICG had an absorption coefficient of 11.5 cm^{-1} at 784 nm and fluoresced over the 790–966 nm spectral range with a peak at 825 nm. The sphere was placed inside a $100\times100\times26$ mm^3 slab of *ex vivo* female breast tissue specimen contained in a transparent plastic box. One of the sides of the box could be moved to uniformly compress and hold the tissue specimen in position. The breast tissue specimen consisted primarily of adipose tissue with small amount of skin and was provided to us by the National Disease Research Interchange under an Internal Review Board approval at the City College of New York. In another experiment to test if the approach could locate a target inside an average-size human female breast, the sphere was placed inside a $250\times250\times50$ mm^3 transparent plastic cell filled with Intralipid-10% suspension in water. The concentration of Intralipid-10% was adjusted to provide transport lengths l_t of ~1 mm at 784 nm and 1.1 mm at 830 nm, which are within the reported range of values for healthy human breast tissues.[19]

A 200 μm optical fiber delivered a 784 nm, 300 mW continuous-wave beam from a diode laser for sample illumination. The beam was collimated to a 1 mm spot onto the entrance face (henceforth referred to as the "source plane") of the slab samples. Multiple source illumination was realized in practice by step scanning the slab samples across the laser beam in an x-y array of grid points using a computer controlled translation stage. The x-y array was 18×15 for the tissue sample and 10×10 for the Intralipid-10% sample, with a step size of 2.5 mm for both the cases. The signal from the opposite face of the sample (henceforth referred to as the "detection plane") was passed through a narrow-band interference filter centered at 830 nm (FWHM ~10 nm, 50% transmission) to block the scattered 784 nm pump light. A camera lens collected the fraction of filtered fluorescence around 830 nm and projected it onto the sensing element of a cooled 16 bit, 1024×1024 pixel charged couple device (CCD) camera. Each illuminated pixel of the CCD camera could be regarded as a detector. For illumination of every scanned point on the source plane, the CCD camera recorded

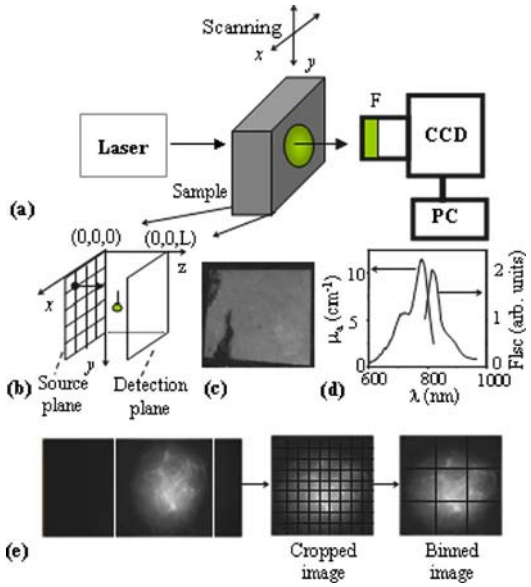

FIG. 1. (a) Schematic diagram of the experimental arrangement (CCD =charge coupled device camera, F=filter, PC=personal computer). (b) An expanded view of the sample input (source) plane and exit (detection) plane showing the grid points in the x-y plane. (c) A photograph of the exit face of the tissue sample. (d) Absorption and fluorescence spectra of the ICG dye solution in water. (e) A typical raw CCD image of the detection plane and how it is cropped and binned for analysis.

the diffusely transmitted 2D fluorescence intensity pattern on the detection plane. A second scan to estimate the average value of $\kappa=\sqrt{3\mu_a\mu_s'}$ (where μ_a and μ_s' are the absorption and scattering coefficients, respectively) of the background medium used a short-pass filter at 750 nm to block the fluores-

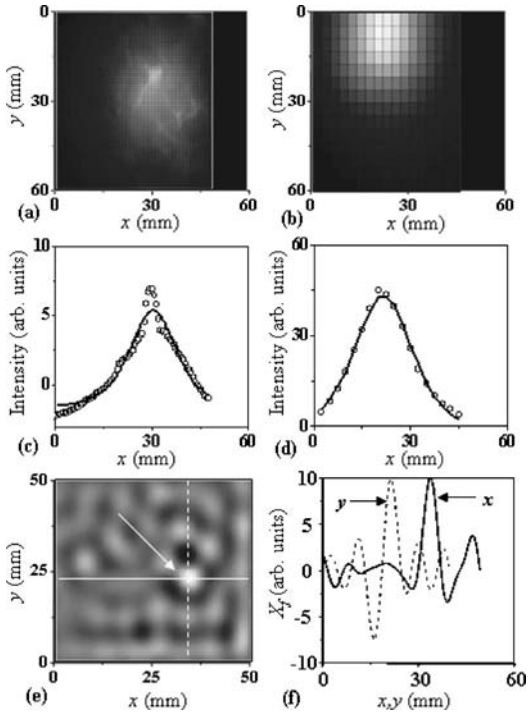

FIG. 2. OPTICA generated fluorescence intensity distribution on (a) the detector and (b) the source planes. [(c) and (d)] Green's function fits to the horizontal spatial profiles through the centers of intensity distributions in (a) and (b), respectively. (e) Cross sectional image at the $z=z_j$ plane. (f) Spatial profiles of the cross sectional image along the x and y directions shown by the white lines in (e).

TABLE I. Comparison of known positions and sizes of the target with OPTICA-determined values.

Samples	Known position (x, y, z) (mm)	Observed position (x, y, z) (mm)	Profile FWHM[a] $(\Delta x, \Delta y)$ (mm)
Breast tissue *ex vivo*	(30, 27, 15)	(30, 27, 16)	(4, 4)
Intralipid-10% in water	(115, 115, 15)	(115, 115, 16)	(12, 12)

[a]The FWHM values should be compared with the inner diameter of 3.2 mm of the sphere.

cence signal and admit a very small fraction of the transmitted excitation light.

Figure 1(b) shows a photograph of the exit surface of the tissue sample. Figure 1(c) presents a typical 2D raw image (fluorescence intensity distribution) of the detection plane recorded by the CCD camera for illumination of a grid point in the source plane. Each raw image is then cropped to select out the information-rich region and binned to enhance the signal-to-noise ratio. All the binned images corresponding to illumination of the grid points in sequence are then stacked and used as input for independent component analysis.

Figures 2(a) and 2(b) present the OPTICA generated intensity distributions on the detector and source planes, respectively, of the tissue sample. The corresponding Green's function fits to horizontal profile through the center of intensity distributions are shown in Figs. 2(c) and 2(d), respectively. The (x,y,z) location of the target center obtained from this analysis is displayed in Table I. The lateral positions (x,y) agree completely, and the axial position agrees within 1 mm of the known values. The cross sectional image obtained using back-projection Fourier transforms in Eq. (5), is shown in Fig. 2(e). Figure 2(f) shows intensity profiles of the cross sectional image along the x and y directions shown by the white dotted lines in Fig. 2(e). The FWHM values of intensity profiles of the cross sectional image, presented in column 4 of Table I, are 4 mm, in good agreement with the known 3.2 mm inner diameter of the fluorescent sphere.

The results of measurements on the same fluorescent sphere embedded in Intralipid-10% suspension in water are also summarized in Table I. Again the lateral positions are in exact agreement, while the axial position agrees within 1 mm. However, the FWHM values of the intensity profiles of the cross sectional image are estimated to be 12 mm each, which is 3.7 times the 3.2 mm inner diameter of the sphere. We attribute this difference primarily to the much larger thickness $(50l_t)$ of the Intralipid-10% sample than that of the tissue sample $(26l_t)$. Spatial resolution decreases rapidly with sample thickness (for the same axial target position) because of the diffuse nature of light propagation through a highly scattering medium. Since the transport lengths (l_t) were comparable and the target was located 15 mm from the source plane for both the samples, the target-detector plane distance in Intralipid-10% sample was more than three times larger than that in the tissue sample, which in turn led to a much higher estimate for the target size. As the incident beam power was limited to 300 mW for both the samples, higher optical thickness resulted in much lower fluorescence signal-to-noise ratio for the Intralipid-10% sample, which in turn contributed to a higher estimate of the target cross section. Substantial improvements in target size estimate are expected if an intensified CCD camera for higher sensitivity, and more incident beam powers are used.

It should be noted that multisource measurements, though crucial for detection of multiple targets, might not be needed for a single target, since the position of the target determines the normalized fluorescence intensity distribution. However, multisource measurements help reduce the deleterious effects of noise and inaccuracy in the estimation of optical properties of the medium and provide better assessment of 3D location even in the case of a single target.

The simpler but important case involving a single target (e.g., a tumor in the breast) was chosen for experimental demonstration. In simulation the approach could locate three targets with one target $\sim 20l_t$ behind another in a $\sim 50l_t$ thick turbid medium. Localization of even more targets is possible and will be presented along with experimental results in a future publication.

In summary, OPTICA can provide rather accurate 3D location of a fluorescent target in a turbid medium and an estimate of its cross section.

This work is supported in part by PSC-CUNY, U.S. Army Medical Research and Materials Command (Grant No. W81XWH-04-1-0461), and NASA COSI program. The authors acknowledge Merlin Brito, David Matten, and Imtiaz Tanveer for technical support.

[1]C. D'Andrea, L. Spinelli, D. Cornelli, G. Valentini, and R. Cubeddu, Phys. Med. Biol. **50**, 2313 (2005).
[2]I. Gannot, V. Chernomordik, A. Garashi, and A. Gandjbakhche, Opt. Lett. **29**, 742 (2004), and Ref. 7 therein.
[3]A. Eidsath, V. Chernomordik, A. Gandjbakhche, P. Smith, and A. Russo, Phys. Med. Biol. **47**, 4079 (2002), and Refs. 2, 5, and 6 therein.
[4]A. B. Thompson, D. J. Hawrysz, and E. M. Sevick-Muraca, Appl. Opt. **42**, 4125 (2003), and Ref. 8 therein.
[5]Sanjay Tyagi, Salvatore A. E. Marras, and Fred Russell Kramer, Nat. Biotechnol. **18**, 1191 (2000).
[6]Alexander D. Klose and Andreas H. Hielscher, Opt. Lett. **28**, 1019 (2003).
[7]M. A. O'Leary, D. A. Boas, X. D. Li, B. Chance, and A. G. Yodh, Opt. Lett. **21**, 158 (1996).
[8]W. Cai, S. K. Gayen, M. Xu, M. Zevallos, M. Alrubaiee, M. Lax, and R. R. Alfano, Appl. Opt. **38**, 4237 (1999).
[9]V. Ntziachristos and R. Weissleder, Opt. Lett. **26**, 893 (2001).
[10]S. R. Arridge, Inverse Probl. **15**, R41 (1999).
[11]A. D. Kim and A. Ishimaru, Appl. Opt. **37**, 5313 (1998).
[12]M. Xu, M. Alrubaiee, S. K. Gayen, and R. R. Alfano, Appl. Opt. **44**, 1889 (2005).
[13]M. Xu, M. Alrubaiee, S. K. Gayen, and R. R. Alfano, J. Biomed. Opt. **44**, 1889 (2005).
[14]J.-F. Cardoso, Proc. IEEE **86**, 2009 (1998).
[15]M. Alrubaiee, M. Xu, S. K. Gayen, M. Brito, and R. R. Alfano, Appl. Phys. Lett. **87**, 191112 (2005).
[16]M. S. Patterson and B. W. Pogue, Appl. Opt. **33**, 1963 (1994).
[17]A. B. Milstein, S. Oh, K. J. Webb, C. A. Bouman, Q. Zhang, D. A. Boas, and R. P. Millane, Appl. Opt. **42**, 3081 (2003).
[18]M. Lax, V. Narayanamurti, and R. C. Fulton, in *Laser Optics of Condensed Matter*, edited by J. L. Birman, H. Z. Cummins, and A. A. Kaplyanskii (Plenum, New York, 1987), pp. 229–237.
[19]H. Heusmann, J. Kölzer, and G. Mitic, J. Biomed. Opt. **1**, 425 (1996).